SUPPORTING MATERIAL

Effects of gel thickness on microscopic indentation measurement of gel modulus

Rong Long[1], Matthew S. Hall[2], Mingming Wu[2], and C. Y. Hui[1]

[1]Field of Theoretical and Applied Mechanics, Sibley School of Mechanical and Aerospace Engineering, Cornell University, Ithaca, NY 14853
[2]Department of Biological and Environmental Engineering, Cornell University, Ithaca, NY 14853

1. Finite Element Simulation of the Microsphere Indentation Experiment.

Deformation of the gel substrate in the microsphere indentation experiments is simulated using a commercial software ABAQUS. Typical lateral dimensions of the gel layer in experiments are on the order of 10 mm, much larger than the gel layer thickness (~ 10^2 μm) and the indenter radius (~ 10^2 μm). As a result, the gel substrate can always be regarded as infinitely wide compared with the size of the microsphere. Therefore, even if the indentation is not carried out in the center of the gel substrate, local gel substrate deformation is still axisymmetric about the vertical axis that goes through the center of the microsphere. This axisymmetry allows us to create a 2D geometry in the finite element simulation, as shown in Fig. S1.

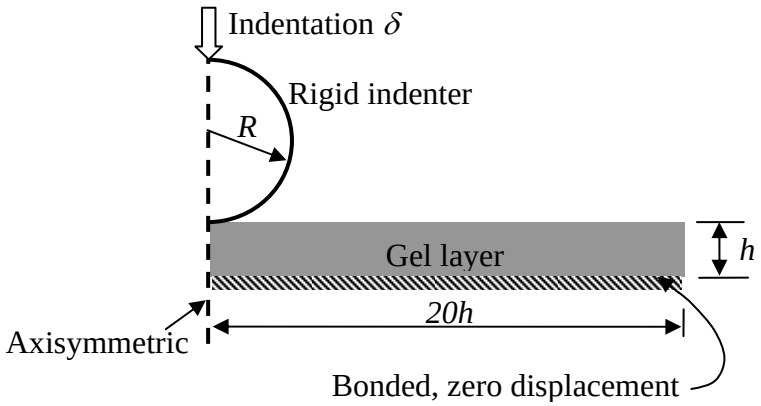

FIGURE S1 Schematic of geometry and boundary conditions in the finite element simulation.

The gel substrate is modeled as a layer of incompressible neo-Hookean solid, with a thickness of h (normalized to 1 in numerical simulation). The initial Young's modulus of the neo-Hookean solid, defined by the modulus when the strain is small, is E (also normalized to be 1 in numerical simulation). To model the infinite extent of the gel layer, its radius is set to be 20h. We have verified that further increasing the gel substrate radius does not affect the numerical results. The indenter is modeled as a rigid sphere of radius R. The outer surface of the indenter and the top surface of the gel substrate are defined to be a contact pair in ABAQUS. Interfacial friction can be controlled by defining the tangential behavior of the interface. We considered two limits of the interfacial friction condition: no-slip condition (infinitely friction) and frictionless (slip) condition (zero friction). It should be noted that the effect of interfacial friction becomes more important as the substrate thickness reduces. A downward vertical displacement δ is imposed on the indenter. The indentation depth δ is increased from 0 to 0.6h incrementally, with each increment being 0.06h. The force F acting on the indenter at every increment is obtained from the finite element results. As shown in Section 3.1, dimensional analysis reveals that

$$F = \frac{16}{9} E\sqrt{R}\delta^{3/2} f\left(\frac{\delta}{h}, \frac{R}{h}\right). \qquad \text{(S1)}$$

To find out the dependence of f on R/h, a series of simulations were carried out where the values of R/h were taken to be 1, 2, 3, 4, 5, 6, 7, 8, 9, 10, 11.5, and 12.7.

We first use a mesh that typically consists of about 3000 elements. The mesh is finer near the indenter (element size ~0.05h) and is coarser far away from the indenter (element size ~0.3h), since deformation of the substrate material far from the indenter vanishes. A representative mesh for $R/h=2$ is shown in Fig. S2A, and Fig. S2B shows the deformed shape of the substrate at an indentation depth of $\delta = 0.6h$. Frictionless condition is used in Fig. S2B.

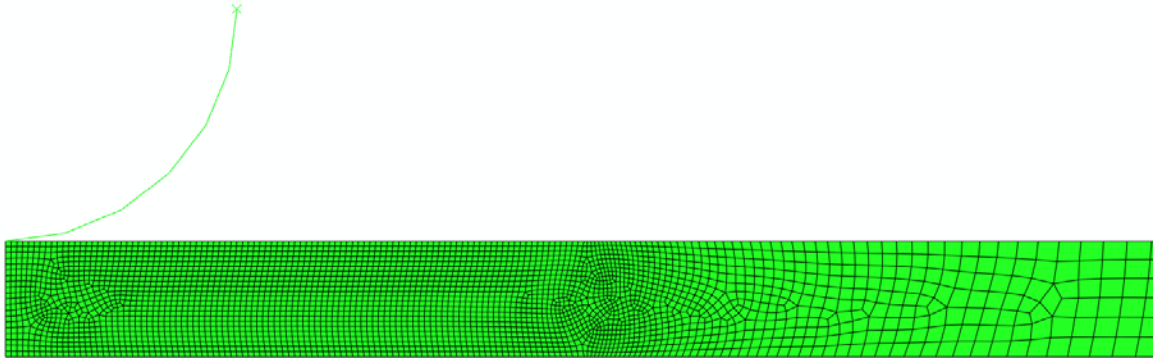

(A)

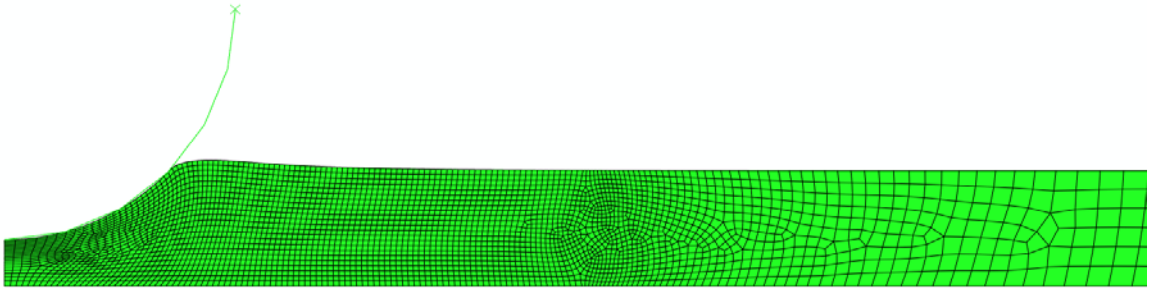

(B)

FIGURE S2 Representative finite element mesh ($R/h = 2$) that consists of about 3000 elements. (A) The undeformed mesh before indentation. (B) The deformed mesh after indentation ($\delta/h = 0.6$). Note that the right end of the substrate layer is not shown in (A) and (B) to better illustrate the mesh near the indenter.

The validity of the finite element results was verified by a convergence test: the finite element results should converge as the mesh size is reduced. We performed the convergence test by using a refined mesh that typically consists of 11,000 elements. The element size is about 0.025*h* near the indenter and is about 0.3*h* far away from the indenter. An example of the convergence test results for $R/h = 2$ with frictionless condition is shown in Fig. S3, where we plot the normalized applied force F/ER^2 versus the normalized indentation depth δ/R for the coarse and refined meshes. Fig. S3 clearly shows the convergence of finite element results. We also plot the prediction of Hertz theory in Fig. S3. Hertz theory predicts a much smaller force *F* than the finite element results, demonstrating the limitations of Hertz theory for thin substrate and large indentation depth.

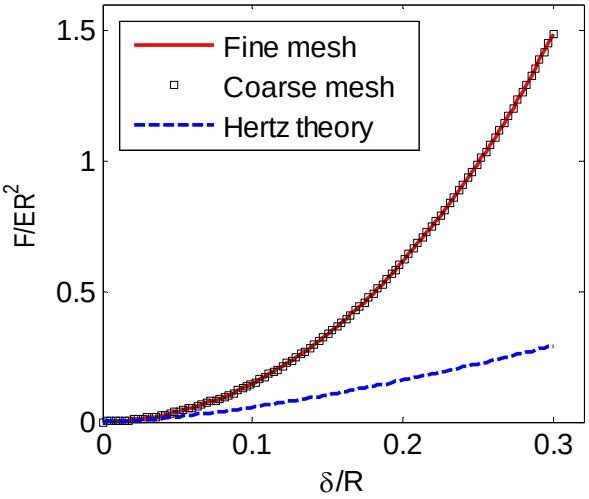

FIGURE S3 The normalized force F/ER^2 versus the normalized indentation depth δ/R for $R/h=2$ (frictionless). The finite element result using fine mesh (red solid line) perfectly agrees with that using coarse mesh (black square). The two meshes are described in the text above. The dashed line is the prediction of Hertz theory, which clearly deviates from the finite element results.

2. Fitting Finite Element Results

Finite element calculations allow us to determine the applied force F for every increment of indentation depth δ. We are interested to determine the correction factor ψ to the Hertz modulus (see Eq. 5 in the paper), where

$$\psi = \frac{E}{E_H} = \frac{16E\delta^{3/2}R^{1/2}}{9F}. \qquad \text{(S2)}$$

For frictionless (slip) conditions, the finite element results of $\psi(\omega)$ using *R/h* from 2 to 12.7 collapsed into a master curve (see Fig. 4A in paper). The same situation occurs for no-slip conditions (see Fig.4B). We first seek an analytical expression that can fit the master curves for both frictionless and no-slip conditions.

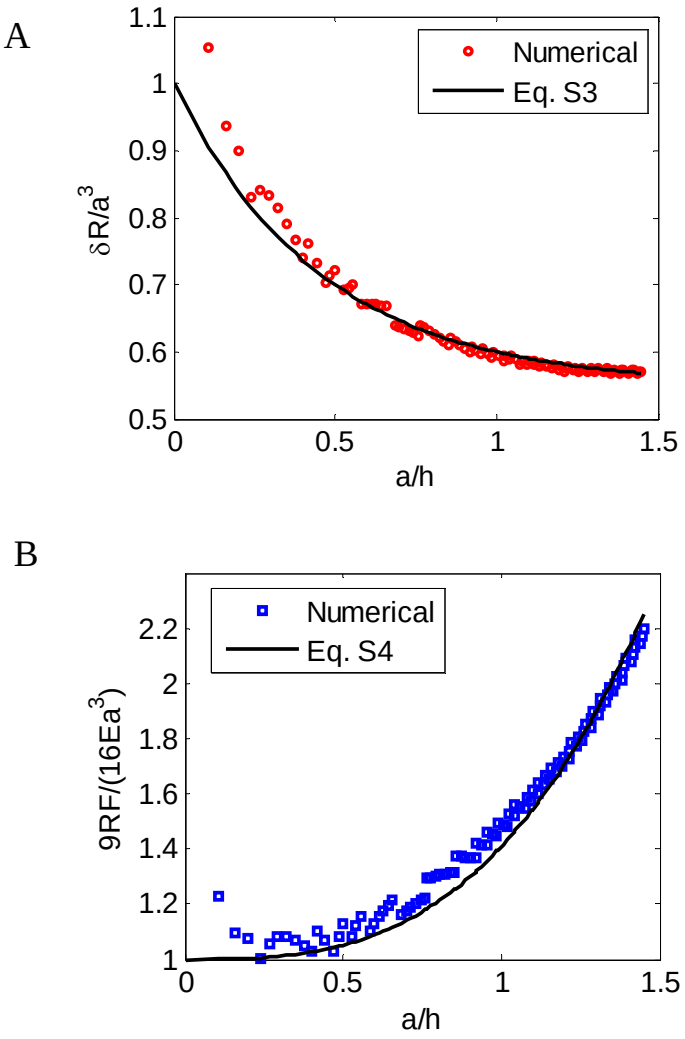

FIGURE S4 Finite element results for $R/h=2$ and frictionless condition. (A) Normalized indentation depth $\delta R/a^2$ versus the normalized contact radius *a/h*. The symbols are finite element results and the solid line is given by Eq. S3. (B) Normalized applied force $9RF/\left(16Ea^3\right)$ versus the normalized contact radius *a/h*. The symbols are finite element results and the solid line is given by Eq. S4.

To motivate the fitting formula, we take the case with $R/h=2$ and frictionless condition as an example. The normalized indentation depth and normalized applied force are plotted as functions of the normalized contact radius *a/h* in Fig. S4A and Fig. S4B, respectively. We found that the numerical results can be well approximated by the following analytical expressions:

$$\delta = \frac{a^2}{R}\left[0.55 + 0.45\exp\left(-2.2a/h\right)\right], \tag{S3}$$

$$F = \frac{16Ea^3}{9R}\left[1 + 0.41(a/h)^3\right], \tag{S4}$$

where a is the contact radius. Note that Hertz theory is recovered as $a/h \to \infty$ in Eq. S3 and S4. Eq. S3 and S4 are very similar to the expressions given in Shull (Ref. 28 in paper) except some numerical constants are changed. We eliminate the contact radius a from Eq. S3 and S4 and find out that

$$\omega = \frac{1}{0.82}\left(-1 + \sqrt{1 + 1.64\frac{\omega}{\psi}}\right)\left[0.55 + 0.45\exp\left(-\frac{2.2}{(0.82)^{1/3}}\left[-1 + \sqrt{1 + 1.64\frac{\omega}{\psi}}\right]^{1/3}\right)\right]^{3/2}, \tag{S5}$$

where $\omega \equiv \left(R\delta/h^2\right)^{3/2}$. Using Eq. S5, it is easy to show that

$$\psi(\omega \to 0) = 1 - 1.49\omega^{1/3} \quad \text{and} \quad \psi\left(\omega \to \infty\right) = \frac{0.4}{\omega + 1}. \tag{S6}$$

Based on the asymptotic behavior given in Eq. S6, we construct a fitting formula for the function $\psi\left(\omega\right)$, i.e.,

$$\psi = \frac{1 + C_1\omega}{1 + C_2\omega^{1/3} + C_3\omega + C_4\omega^2}, \tag{S7}$$

where C_i (i=1 to 4) are numerical constants and can be determined by fitting the finite element results to Eq. S7. The best fit we found for both no-slip and frictionless condition is: $C_1 = 2.3$, $C_2 = 1.15$, $C_3 = 9.5$, and $C_4 = \beta^*$, where β^* is 9.288 for no-slip condition and is 4.212 for frictionless condition. Comparison of the analytical expression (Eq. 8) and the finite element results are shown in Fig. 4A and 4B in the paper.

When *R/h* is less than 2, the correction factor ψ is a function of both *δ/h* and *R/h*, instead of solely depending on a single parameter ω (see Fig. 3 in paper). However, we found that Eq. S7 can still be used to fit finite element results for different *R/h*. Specifically, the following formula is used:

$$E/E_H = \psi = \frac{1 + 2.3\omega}{1 + 1.15\omega^{1/3} + \alpha\omega + \beta\omega^2}. \tag{S8}$$

The numerical coefficients α and β are functions of *R/h*, and were obtained by fitting Eq. S8 to finite element results for different *R/h* from 0.5 to 12.7 (with δ/h up to 0.6). For example, values of α and β for frictionless (slip) condition are shown in Fig. S5A and S5B, respectively. The solid lines in Fig. S5A and S5B are obtained using Eq. 7a and Eq. 7b in paper, which can well approximate numerical results of α and β, as shown in the figure. Similarly, we found that, for no-slip condition, α and β can be well approximated by Eq. 7c and Eq. 7d in paper.

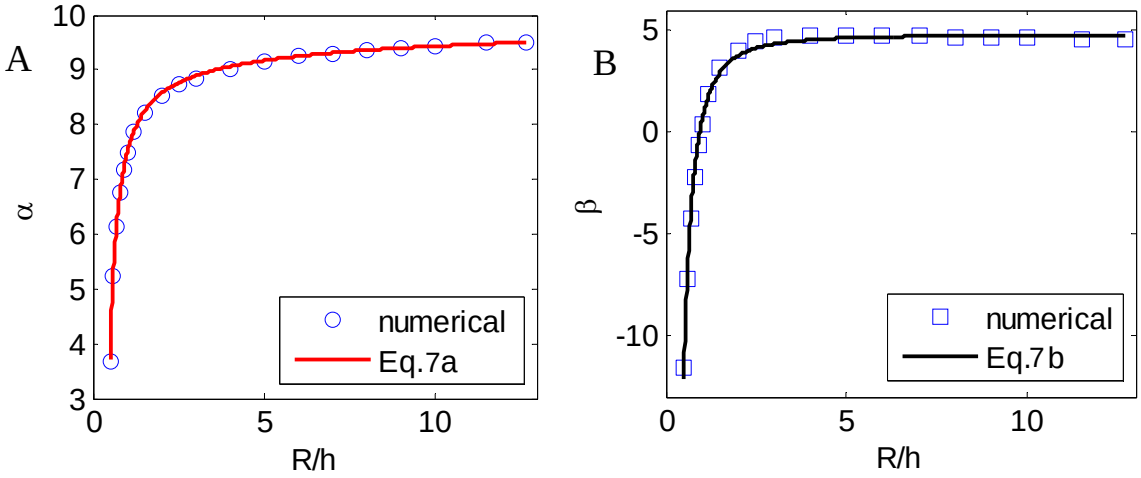

FIGURE S5 (A) Numerical results of α in Eq. S8 for frictionless interface (circle). The solid line is obtained using Eq.8a in paper. (B) Numerical results of β in Eq. S8 for frictionless interface (square). The solid line is obtained using Eq.8b in paper.

Although obtained by fitting finite element data for *R/h* from 0.5 to 12.7, the correction factor (Eq. 6 in paper) can be applied to smaller *R/h*. For example, for the case of frictionless condition (slip) and *R/h* = 0.3, the maximum error made by Eq. 6 relative to the finite element results is about 3% for δ/h up to 0.3 (see Fig. S6). In other words, Eq. 6 applies to the regime of *R/h* = 0.3 and $\delta/h \le 0.3$. Therefore, the region of applicability of Eq. 6 is extended to $\delta/h \le \min(0.6, R/h)$ and $0.3 \le R/h \le 12.7$.

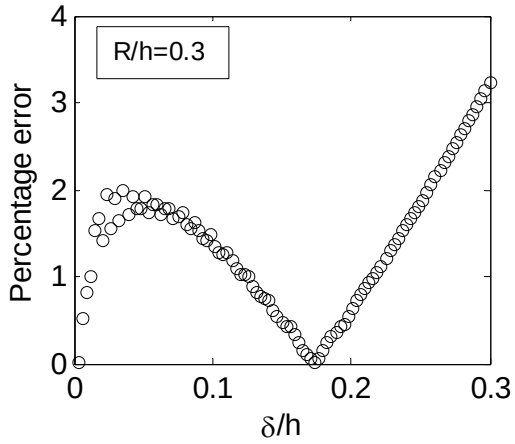

FIGURE S6 Percentage error (= $100\times\left|\psi-\psi_{FEM}\right|/\psi_{FEM}$, where ψ is given by Eq. 6 and ψ_{FEM} is the finite element result of correction factor) made by Eq. 6 for $R/h=0.3$ and δ/h up to 0.3. The maximum relative error is about 3%.

3. Effect of adhesion

The JKR theory has been used extensively to characterize the surface energy of soft materials (see Ref. 36 in paper). Briefly, the JKR theory is an extension of Hertz theory, in that it accounts for adhesion by including the effect of attractive surface forces that act between two contacting surfaces. These surface forces are modeled by adding a tensile stress distribution to the usual compressive stress of the Hertz theory. The magnitude of this tensile stress distribution is determined by the work of adhesion, *W*, of the materials in contact. To summarize, a correction term due to adhesion is subtracted from the Hertz force and displacement, resulting in

$$F=F_H-2a^{3/2}\sqrt{8\pi E_{JKR}W/3} \tag{S9}$$

$$\delta=\delta_H-\sqrt{\frac{3\pi Wa}{2E_{JKR}}}, \tag{S10}$$

where F_H,δ_H are the force and indentation depth predicted by Hertz theory, and *a* is the radius of the contact region in the presence of adhesion. E_{JKR} is the Young's modulus of the substrate which is infinitely thick, similar to that in Hertz theory. The subscript "JKR"

is used to distinguish from the modulus E in the paper that accounts for finite thickness effect but neglects the adhesion. Eq. S9 states that a smaller compressive force (indentation depth) is needed to bring two adhering spheres into the same amount of contact. The Young's modulus E_{JKR} can be obtained by eliminating the contact radius in Eq. S9 and Eq. S10 using $F_H = 16E_{JKR}a^3/(9R)$ and $\delta_H = a^2/R$, i.e.,

$$\frac{E_{JKR}}{E_H} = \left(\frac{3\pi RW}{2F}\right)\left(1+\sqrt{1+\frac{2F}{3\pi RW}}\right)^{1/2}\left[-\frac{1}{3}+\sqrt{1+\frac{2F}{3\pi RW}}\right]^{3/2}, \qquad \text{(S11)}$$

where $E_H = 9F/\left(16\sqrt{R}\delta^{3/2}\right)$ is the modulus obtained using Hertz theory. The left hand side of Eq. S11 is the correction factor for adhesion. The accuracy of modulus determined using Hertz theory can be quantified by plotting E_{JKR}/E_H against $F/F_{pull-off}$ (see Fig.S7), where $F_{pull-off} = 3\pi RW/2$ is the pull-off force in JKR theory (Ref. 36 in paper). As shown in Fig. S7, E_{JKR}/E_H can be much greater than 1 for small $F/F_{pull-off}$ or small indentation. This result shows that the actual modulus can be many times larger than the modulus determined using Hertz theory, as pointed out by Frey *et al.* (Ref.22 in paper).

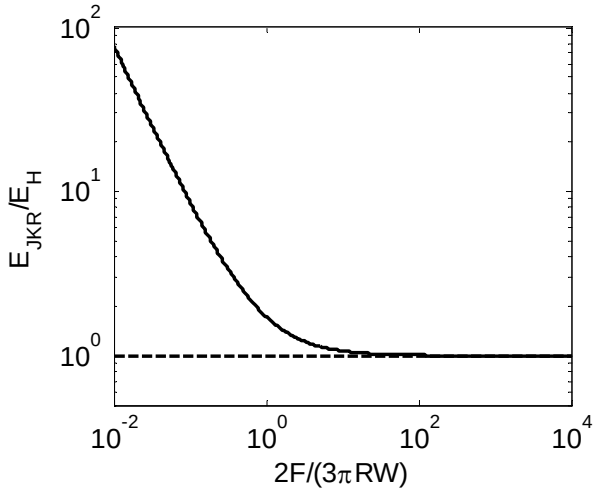

FIGURE S7 Log-Log plot of E_{JKR}/E_H versus the dimensionless force $2F/(3\pi RW)$. The dashed lines serves as a reference where the value of E_{JKR}/E_H is exactly 1.